Front. Earth Sci. 2014, 8(3): 427–438
DOI 10.1007/s11707-014-0412-4

RESEARCH ARTICLE

A simplified physically-based algorithm for surface soil moisture retrieval using AMSR-E data

Jiangyuan ZENG[1,2], Zhen LI[1], Quan CHEN (✉)[1], Haiyun BI[1,2]

1 Key Laboratory of Digital Earth Science, Institute of Remote Sensing and Digital Earth, Chinese Academy of Sciences, Beijing 100094, China
2 University of Chinese Academy of Sciences, Beijing 100049, China

© Higher Education Press and Springer-Verlag Berlin Heidelberg 2014

Abstract A simplified physically-based algorithm for surface soil moisture inversion from satellite microwave radiometer data is presented. The algorithm is based on a radiative transfer model, and the assumption that the optical depth of the vegetation is polarization independent. The algorithm combines the effects of vegetation and roughness into a single parameter. Then the microwave polarization difference index (MPDI) is used to eliminate the effects of surface temperature, and to obtain soil moisture, through a nonlinear iterative procedure. To verify the present algorithm, the 6.9 GHz dual-polarized brightness temperature data from the Advanced Microwave Scanning Radiometer (AMSR-E) were used. Then the soil moisture values retrieved by the present algorithm were validated by in-situ data from 20 sites in the Tibetan Plateau, and compared with both the NASA AMSR-E soil moisture products, and Soil Moisture and Ocean Salinity (SMOS) soil moisture products. The results show that the soil moisture retrieved by the present algorithm agrees better with ground measurements than the two satellite products. The advantage of the algorithm is that it doesn't require field observations of soil moisture, surface roughness, or canopy biophysical data as calibration parameters, and needs only single-frequency brightness temperature observations during the whole retrieval process.

Keywords passive microwave remote sensing, soil moisture, inversion, AMSR-E, SMOS

1 Introduction

Soil moisture plays a critical role in land-atmosphere interactions. It has been proven that global soil moisture observations are very useful in hydrology, climatology, agriculture, and meteorology (Jackson et al., 1987; Saha, 1995; Shi et al., 2006; Wang and Qu, 2009; Du, 2012). Therefore, it is very important to obtain a wide range of soil moisture information both temporally and spatially. In-situ soil moisture measurements are usually point-based observations, hence they are not sufficient to fully capture the spatial and temporal variability of soil moisture on a large scale. In contrast, passive microwave sensors can provide earth observation data with a spatial resolution of dozens of kilometers. Thus, they are very suitable for soil moisture monitoring at large scales (Mao et al., 2008; Mladenova et al., 2011). Furthermore, passive microwave sensors have their own advantages for soil moisture measurement: (a) capable of working both day and night, (b) able to penetrate cloud layers, and less affected by atmospheric conditions, (c) directly related to soil moisture through soil permittivity, and (d) less sensitive to land surface roughness and vegetation cover compared to active microwave sensors (Shi et al., 2008; Draper et al., 2009).

The physical basis of using passive microwave remote sensing technology for soil moisture monitoring is that microwave brightness temperature is highly related to the soil dielectric constant, which is mainly determined by soil moisture (Jackson, 1993; Njoku et al., 2003). Besides, brightness temperature is also affected by many other factors, such as vegetation cover, soil and vegetation temperatures, surface roughness, and soil texture (Njoku and Entekhabi, 1996; Wigneron et al., 2003). These perturbing factors bring uncertainties into the relationship between brightness temperature and soil moisture, thereby decreasing the accuracy of soil moisture estimation. Therefore, it is very important to eliminate the effects of these factors during the soil moisture inversion process. Additionally, lower frequencies respond to a deeper soil layer and are less attenuated by atmosphere and vegetation, hence the low-frequency microwave range of 1–3 GHz (i.e., L-band) is considered optimal for soil moisture detection (Njoku and Entekhabi, 1996).

Received May 27, 2013; accepted September 10, 2013

E-mail: qchen@ceode.ac.cn

Currently, the lowest frequency radiometer in orbit is the Microwave Imaging Radiometer with Aperture Synthesis (MIRAS) mounted on the Soil Moisture and Ocean Salinity (SMOS) satellite, which provides multi-angular observations of brightness temperature at 1.4 GHz (Kerr et al., 2001). Unfortunately, the SMOS brightness temperature measurements have been severely affected by Radio Frequency Interference (RFI) in some parts of the world (Skou et al., 2010; Anterrieu and Khazaal, 2011; Dente et al., 2012a). Compared with the SMOS satellite, the Advanced Microwave Scanning Radiometer (AMSR-E) has the advantage of being less affected by RFI and has been proven to have substantial potential in soil moisture estimation (Santi et al., 2012). Thus, it is becoming one of the most important passive microwave sensors for soil moisture monitoring.

The AMSR-E sensor measures brightness temperatures at six dual-polarized frequencies in the range of 6.9–89 GHz (Njoku et al., 2003). Several preeminent soil moisture inversion algorithms have been developed for the AMSR-E sensor (Jackson, 1993; Njoku et al., 2003; Koike et al., 2004; Njoku and Chan, 2006; Paloscia et al., 2006; Owe et al., 2008; Santi et al., 2012). NASA adopted the algorithm developed by Njoku et al. (2003). The algorithm performs an iterative minimization of the root mean square error (RMSE) between model simulations and satellite observations for three parameter (soil moisture, vegetation water content, and soil temperature) retrievals. Unfortunately, this algorithm has the problem of possible multiple solutions and is also time consuming. Njoku and Chan (2006) modified its earlier version by using a global regressive method. The algorithm uses the microwave polarization difference index (MPDI) of AMSR-E brightness temperatures at 10.65 and 18.7 GHz to account for the effects of vegetation and roughness. Soil moisture is estimated using the deviation of MPDI at 10.65 GHz from a baseline value. However, some studies have suggested that uncertainties may arise when applying this method in some areas, especially outside of the United States (U.S) (Draper et al., 2009; Zhang et al., 2011). The land parameter retrieval model (LPRM) developed by Owe et al. (2008) is another prominent method for soil moisture estimation. The unique feature of this approach lies in the way that vegetation optical depth is derived. In the algorithm, vegetation optical depth is expressed as a function of the soil dielectric constant and the MPDI. Therefore, it can solve vegetation optical depth automatically and avoid reliance on additional vegetation data sets (Meesters et al., 2005). However, the surface roughness parameter is assumed to be globally constant in the model, which is inconsistent with the actual surface and may cause big errors during the inversion process (Jackson et al., 2010). Jackson et al. (2010) compared four typical soil moisture inversion algorithms using four soil moisture networks in the U.S. The results show that the single-channel algorithm (Jackson, 1993) has the highest accuracy. But this algorithm needs more auxiliary parameters, such as the vegetation water content and surface roughness data sets. The vegetation water content is calculated by the normalized difference vegetation index (NDVI) from optical data (Jackson et al., 1999). However, optical sensors are often influenced by clouds and cannot work at night or on rainy days, which greatly limits the use of this method.

In this study, a simplified physically-based algorithm was developed for surface soil moisture retrieval using passive microwave radiometer data. The algorithm is based on a radiative transfer model and the assumption that the vegetation optical depth is polarization independent. Then, the soil moisture retrieved by the present algorithm, using the 6.9 GHz dual-polarized brightness temperatures from AMSR-E, were validated by ground measurements collected from the Maqu soil moisture monitoring network, and were also compared with both the NASA AMSR-E soil moisture products and SMOS soil moisture products. The advantage of this algorithm is that it takes into account the influence of both vegetation and surface roughness on surface radiation, and no field observations of roughness, soil moisture, or canopy biophysical properties for calibration purposes are necessary during the whole retrieval process. Since the method is physically-based with no regional dependence, and needs only single frequency brightness temperature observations for soil moisture inversion, it may also be applied to soil moisture inversion in the SMOS satellite mission, and the Soil Moisture Active/Passive (SMAP) mission (Entekhabi et al., 2010), with slight adjustments.

2 Methodology

The algorithm is based on a zero-order radiative transfer model, usually called τ–ω model (Mo et al., 1982). In this model, the effects of atmospheric moisture and multiple scattering in the vegetation layer are neglected, and the brightness temperature T_{Bp} of a soil and vegetation layer is the sum of three terms: (1) soil emission attenuated by the canopy, (2) the direct vegetation emission, and (3) the vegetation emission reflected by the soil and attenuated by the canopy, which can be expressed as

$$\begin{aligned} T_{Bp} =& (1-R_{sp})T_s\exp(-\tau_p) + (1-\omega)T_c[1-\exp(-\tau_p)] \\ &+ (1-\omega)T_c[1-\exp(-\tau_p)]R_{sp}\exp(-\tau_p), \end{aligned} \tag{1}$$

where the subscript p represents the vertical or horizontal polarization, R_{sp} is the topsoil effective reflectivity, T_s and T_c are the temperatures of the soil and vegetation canopy, respectively, τ_p is the vegetation optical depth along the observation path used to parameterize the vegetation

attenuation properties, and ω is the single scattering albedo of the vegetation used to parameterize the scattering effects within the canopy layer.

Although Roy et al. (2012) pointed out that ω should not be zero in the forest coverage area at AMSR-E frequencies; its effects are often neglected under light-vegetation conditions (Jackson, 1993). For simplicity, it is assumed that ω is equal to zero (Jackson, 1993; Van de Griend and Owe, 1994; Njoku and Chan, 2006). τ_p is also supposed to be polarization independent, which is widely accepted at satellite scales (Njoku et al., 2003; Njoku and Chan, 2006; Owe et al., 2008). Furthermore, the soil and vegetation temperatures are assumed to be equal and represented as T, which is more reasonable in the nighttime. Then, Eq. (1) can be simplified as

$$T_{Bp} = T[1 - R_{sp}\exp(-2\tau)]. \tag{2}$$

The effective reflectivity (R_{sp}) from rough soil surface is very difficult to obtain at a satellite scale directly. Thus, some researchers have proposed various methods based on different roughness models to correct the effects of surface roughness on surface reflectivity (Shi et al., 2006; Chen et al., 2010; Guo et al., 2013). However, all of these methods can only be applied to bare ground surface and cannot be applied directly to vegetation coverage areas. Recently, Hong (2010) proposed a method to estimate small-scale roughness, but further verification of the validity and reliability of this method is needed (Guo et al., 2013). In our study, the Q/H model (Wang and Choudhury, 1981) was used to parameterize the topsoil effective reflectivity (R_{sp}). The Q/H model is expressed as

$$R_{sp} = [(1-Q)R_{op} + QR_{oq}]\exp(-h), \tag{3}$$

where p and q denote orthogonal polarizations, the parameter Q, which is also called the polarization mixing parameter, describes the energy emitted in the orthogonal polarizations that results from the surface roughness effect, and h describes the effect of surface roughness, leading to a decrease in the effective reflectivity. By inserting Eq. (3) into Eq. (2) and then combining the coefficients, we can obtain (Saleh et al., 2006)

$$T_{Bp} = T[1 - R'_{sp}\exp(-2\tau - h)], \tag{4}$$

where R'_{sp}=(1–Q)R_{op}+ QR_{oq}. Njoku and Chan (2006) took Q as a fixed global calibration factor and left h to incorporate the roughness spatial variability at C/X/Ku-band of the AMSR-E sensor. In this study, the same fixed value of Q (0.174) at 6.9 GHz (C-band) was adopted. Thus, according to the Fresnel equations, R'_{sp} is only related to the soil dielectric properties at a specific incident angle. The Hallikainen empirical model (Hallikainen et al., 1985) was used to convert the soil dielectric constant into soil moisture. Therefore, if the soil texture data are known, R'_{sp} can be expressed as a function of soil moisture (i.e., R'_{sp}= $f(sm)$) at a given frequency and incident angle. In Eq. (4), the exponential attenuation effects of vegetation and roughness are grouped into a single parameter (i.e., exp (–2τ–h)). Our purpose is to express the single parameter as a form which is related to soil moisture, so as to avoid dependence on the auxiliary data of vegetation and roughness, as well as to avoid making unreliable assumptions. In addition, let exp(–2τ–h) = a. Then, at a given frequency with H and V polarization, Eq. (4) can be expressed as

$$T_{Bh} = T(1 - R'_{sh}a), \tag{5}$$

$$T_{Bv} = T(1 - R'_{sv}a). \tag{6}$$

By combining Eq. (5) and Eq. (6), the single parameter a can be derived

$$a = \frac{T_{Bv} - T_{Bh}}{T_{Bv}R'_{sh} - T_{Bh}R'_{sv}}. \tag{7}$$

Hence, the single parameter a is expressed as a function of R'_{sp} with observed brightness temperature. By inserting Eq. (7) into Eq. (5) and Eq. (6), the H and V polarized brightness temperatures at a given frequency can be obtained

$$T_{Bh} = T\left(1 - R'_{sh}\frac{T_{Bv} - T_{Bh}}{T_{Bv}R'_{sh} - T_{Bh}R'_{sv}}\right), \tag{8}$$

$$T_{Bv} = T\left(1 - R'_{sv}\frac{T_{Bv} - T_{Bh}}{T_{Bv}R'_{sh} - T_{Bh}R'_{sv}}\right). \tag{9}$$

Thus, according to Eq. (8) and Eq. (9), the differences between the H and V polarized brightness temperatures are only influenced by soil moisture and surface temperature. Additionally, the MPDI (Becker and Choudhury, 1988; Paloscia and Pampaloni, 1988) is often used to remove the temperature dependence of the emitting layer on T_{Bp} (Owe et al., 2008). The MPDI is defined as

$$\mathrm{MPDI} = \frac{T_{Bv} - T_{Bh}}{T_{Bv} + T_{Bh}}. \tag{10}$$

By inserting Eq. (8) and Eq. (9) into Eq. (10), we can obtain the simulated MPDI (i.e., MPDI_{sim}), which is related to R'_{sp} and observed dual-polarized brightness temperature. Thus, the MPDI_{sim} can be expressed as a function of soil moisture with known soil texture at a given frequency. This means that soil moisture is the only unknown parameter in the MPDI_{sim} (with known soil texture under AMSR-E configurations). Finally, a non-linear iterative procedure was performed to minimize the absolute value of the difference between the simulated and observed MPDI (i.e., $abs(\mathrm{MPDI}_{obs}–\mathrm{MPDI}_{sim})$= min) in order to calculate surface soil moisture. The flow chart of the methodology is illustrated in Fig. 1.

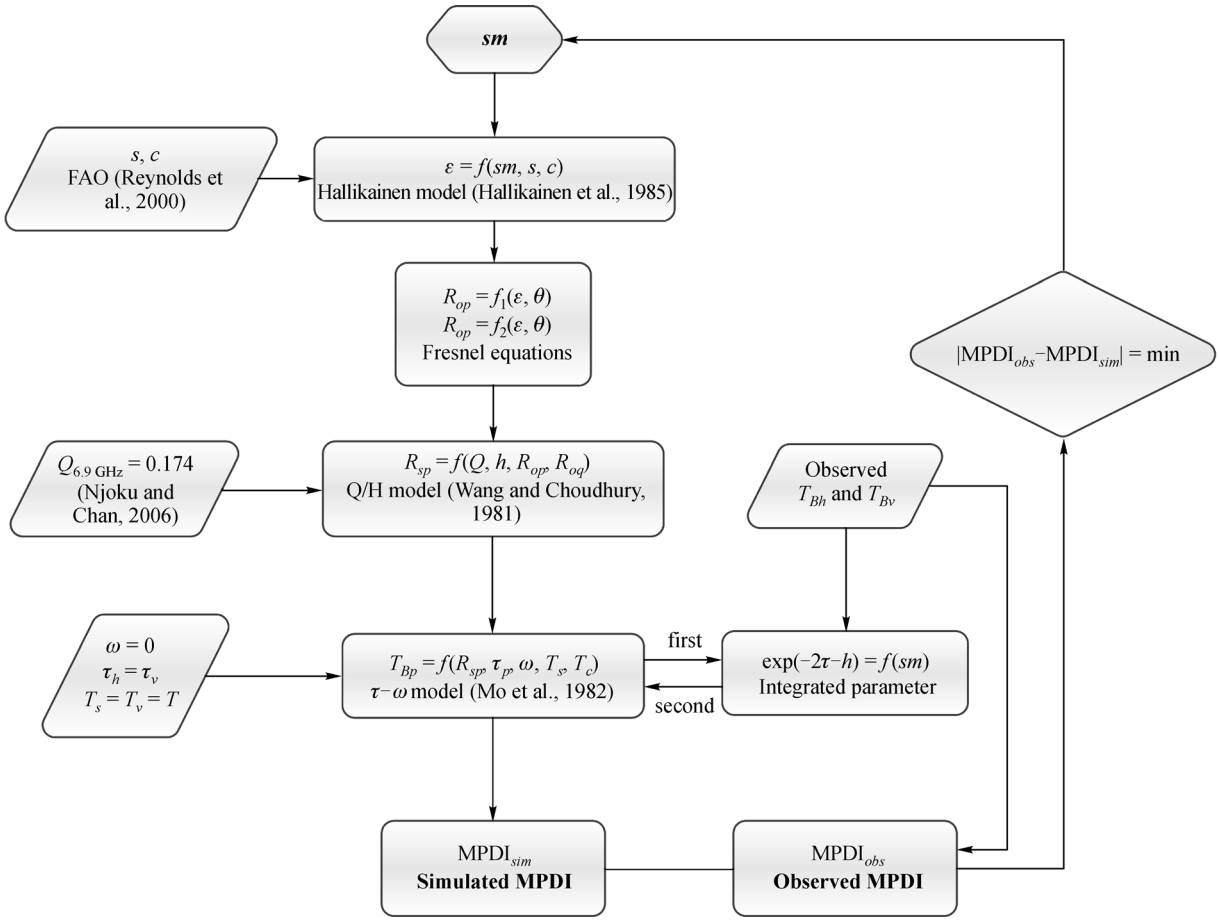

Fig. 1 The flow chart of the proposed algorithm for surface soil moisture retrieval.

3 Experimental data

3.1 AMSR-E data

For this study, the AMSR-E level 3 data products from the National Snow and Ice Data Center (NSIDC) were used. The brightness temperature data had been re-sampled to 25 km×25 km with a global EASE-GRID projection. Due to the ability to maximize vegetation and soil penetration and minimize atmospheric effects than the higher frequencies of AMSR-E, as well as no apparent RFI at C-band over the Tibetan Plateau (Njoku et al., 2005), the dual-polarized brightness temperatures at 6.9 GHz were used for soil moisture inversion. The NASA AMSR-E soil moisture products were used for comparison. In addition, Lacava et al. (2013) also conducted a very detailed investigation of AMSR-E C-band RFI over the world. In their nine year study (from June 2002 to May 2011) of AMSR-E data they found that a large part of North America, and several zones in India, South America, Japan, and Europe are affected by RFI, but there is no apparent RFI at C-band over the Tibetan Plateau, which is in agreement with Njoku et al.'s work (2005). Moreover, due to the greater stability of nighttime surface temperatures, which makes the assumption that the vegetation temperature is equal to soil temperature more reasonable, only nighttime data (corresponding to the AMSR-E descending pass) were used in the study.

3.2 SMOS data

The SMOS satellite was launched successfully on November 2, 2009. It can provide global maps of soil moisture and ocean salinity, and thus has become a useful tool for monitoring key elements of the global water cycle (Jacquette et al., 2010). The SMOS Level 3 daily soil moisture products from April 1 to July 31, 2010 were used in this study. The projection of these products is consistent with that of the AMSR-E, namely the EASE-GRID projection with a spatial resolution of 25 km×25 km (Berthon et al., 2012). For the purpose of reducing the temperature difference between the vegetation canopy and topsoil, the SMOS ascending soil products corresponding to morning time, (6 a.m.) were used for comparison.

3.3 In-situ data

The Tibetan Plateau has a strong influence on the climatic system of Asia due to its high average elevation of 4,000

m. Soil moisture plays a critical role in the water cycle and climate of this area, thus affecting the monsoon system and precipitation patterns (Xie et al., 2010; Dente et al., 2012b). The Maqu soil moisture monitoring network (Su et al., 2011), which is located in the north-eastern part of the Tibetan Plateau, was selected for validation in this study. The network, shown in Fig. 2, covers an area of approximately 40 km×80 km and consists of 20 sites. The 20 sites recorded soil moisture and soil temperature from July 1, 2008 to July 31, 2010 at different depths (from 5 to 80 cm below surface) and a temporal resolution of 15 minutes (Su et al., 2011). These sites are distributed in the large valley of the Yellow River and the surrounding hills, and are covered by short grassland uniformly.

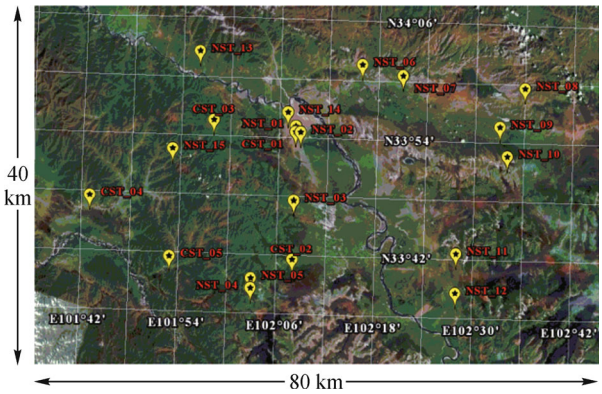

Fig. 2 Location of the 20 sites of the Maqu soil moisture monitoring network. CST and NST represent the names of these sites.

Figure 3 shows the temporal variations of averaged NDVI within the Maqu network region from July 1, 2008 to July 31, 2010, which shows the apparent growth variations of the vegetation during the period. The NDVI data were obtained from Free Vegetation Products (http://www.vito-eodata.be), resulting from 10 days of SPOT-4 acquisitions with a resolution of 1 km. The average NDVI during the growing season, from April to October, is about 0.5. The NDVI averages around 0.18 from November to March. The daily averaged soil moisture, measured at 5 cm at all 20 sites, provided the in-situ soil moisture measurements for validation of the soil moisture retrieved by the present algorithm, and the two satellite soil moisture products (i.e., NASA AMSR-E and SMOS), which were also averaged over all grids within the Maqu network. A number of studies have been conducted to determine the soil freeze-thaw status using passive microwave measurements (Jin et al., 2009; Zhao et al., 2011a), but in this study we determined the soil freeze-thaw status using the observed surface soil temperature.

The surface soil temperature is below 0°C from November to April in the study area. The soil is frozen and the soil dielectric model is no longer applicable in this case (Hallikainen et al., 1985). Therefore, observations during this period were excluded from this study. The soil texture data used in this study were obtained from the Food and Agriculture Organization (FAO) of the United Nations (Reynolds et al., 2000). Figure 4 shows the temporal variations of averaged soil moisture and soil temperature at 5 cm at all of the 20 sites during the entire period.

4 Results and discussion

Due to differences in both spatial resolution and vertical resolution between satellite and in-situ data, it makes more sense to compare time series trends than specific values (Owe et al., 2008). A detailed long time series comparison conducted during this study is presented in Fig. 5, which shows the temporal variations of soil moisture retrieved by the inversion algorithm (Algorithm_SM), the NASA AMSR-E soil moisture products (NASA_SM), and the in-situ average soil moisture at 5 cm (In-situ_SM), from July 1, 2008 to October 31, 2008, April 1, 2009 to October 31, 2009, and April 1, 2010 to July 31, 2010, respectively. The SMOS soil moisture products (SMOS_SM) from

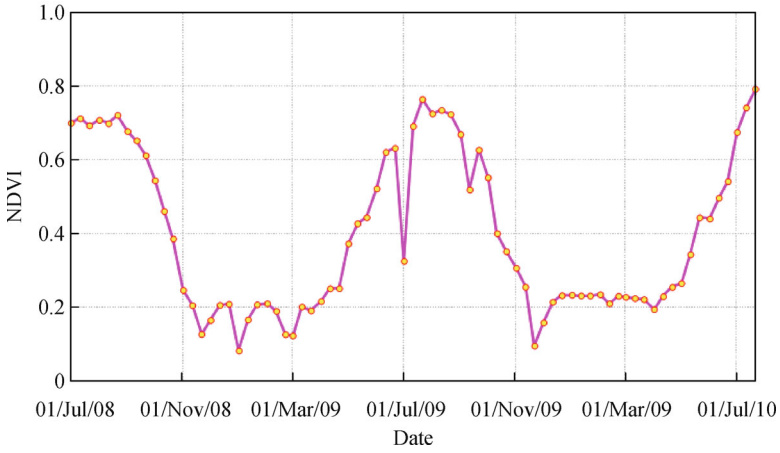

Fig. 3 Temporal variations of averaged NDVI at the Maqu network region during the entire period.

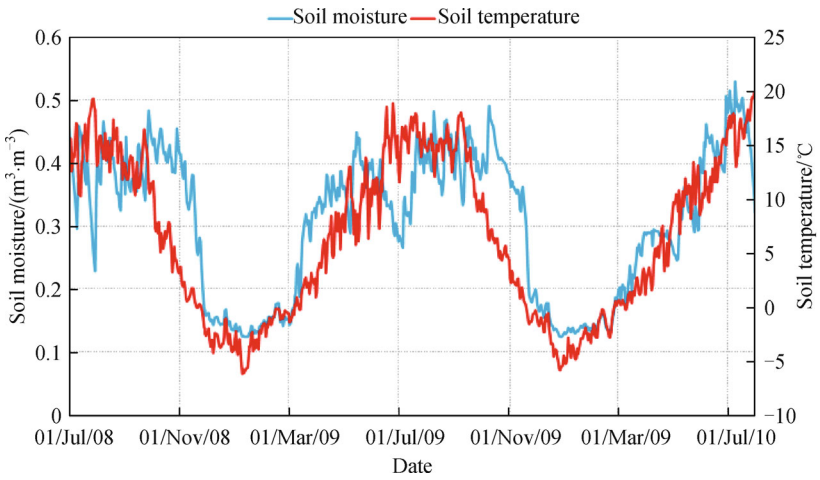

Fig. 4 Temporal variations of averaged soil moisture and soil temperature at 5 cm at the Maqu network region during the entire period.

April 1, 2010 to July 31, 2010 were also displayed in Fig. 5 (c).

The Maqu network is in a cold humid climate with frequent rainfall events during April to October (Dente et al., 2012b). This can be seen from the precipitation data presented in Fig. 5, which shows the apparent temporal variations in soil moisture. The temporal behavior of the Algorithm_SM generally agrees well with the In-situ_SM during the entire period, except for May 2009 to July 2009, whereas the NASA_SM displays almost constant values around 0.15, and it cannot capture the temporal variation trends of the ground soil moisture all of the time. The lack of soil moisture dynamics within the NASA retrievals is consistent with previous studies (Wagner et al., 2007; Rüdiger et al., 2009). Although SMOS products exhibit variability as time changes, they do not show any trend, and obviously overestimate the temporal variations in soil moisture, resulting in a serious underestimation or overestimation of soil moisture during certain periods (e.g., underestimation in April, and overestimation in May). The standard deviation (STD) of the Algorithm_SM, NASA_SM, SMOS_SM, and In-situ_SM, which shows the variability in these data, is shown in Table 1. It further confirms that the Algorithm_SM matches better with in-situ soil moisture data than both the NASA_SM and SMOS_SM with temporal variation.

Figure 6 is the histogram of the distribution of mean absolute error (MAE) between in-situ soil moisture and the three soil moisture retrievals. The horizontal axis represents the interval range of the MAE, and the vertical axis represents the overall proportion of these errors. It is clear that the Algorithm_SM is closest to the In-situ_SM. About 40% of the MAE values between retrievals and measurements are less than 0.05 $m^3 \cdot m^{-3}$, and most of them are within 0.1 $m^3 \cdot m^{-3}$. The SMOS official algorithm follows, with nearly 40% of the values of the MAE between retrievals and measurements being less than 0.1 $m^3 \cdot m^{-3}$. The NASA official algorithm performs the worst. Using the NASA official algorithm, 70% of the MAE values were larger than 0.2 $m^3 \cdot m^{-3}$, indicating that this algorithm introduces large errors when applied in the Maqu network region.

The scatter plots shown in Fig. 7 and the error statistics listed in Table 1 also indicate that the soil moisture retrieved by the present algorithm is most consistent with in-situ data. Results obtained using the Algorithm_SM are closest to the 1 : 1 line and present a better fit to the in-situ data than the NASA_SM, and SMOS_SM, with the smallest RMSE lower than 0.1 $m^3 \cdot m^{-3}$ at any period. The NASA algorithm appears to underestimate soil moisture throughout the period with the largest RMSE of 0.235 $m^3 \cdot m^{-3}$. This conclusion is consistent with Zhao et al. (2011b), who also found that the NASA soil moisture products were obviously lower than the ground soil moisture in the Tibetan Plateau. The SMOS_SM deviates far from the 1 : 1 line with a relatively large RMSE of 0.140 $m^3 \cdot m^{-3}$. The Bias, MAE, and RMSE, displayed in Table 1 further demonstrate a comprehensive improvement in soil moisture estimation using the present algorithm in comparison with the NASA soil moisture products and the SMOS soil moisture products.

The poor accuracy of the satellite-derived soil moisture products (i.e., AMSR-E, SMOS) over the Tibetan plateau, particularly in the Maqu network region, is consistent with previous studies (Su et al., 2011; Dente et al., 2012a; Chen et al., 2013). The NASA_SM's exhibiting such a large error may be caused by the use of a global empirical regression algorithm. The coefficients in the algorithm are mainly calibrated in the U.S, hence may not be appropriate in the Tibetan Plateau (Lu and Shi, 2012). The errors of SMOS products may be derived from three parts: (a) the inaccurate surface temperature provided by the European Centre for Medium-Range Weather Forecasts (ECMWF) model, (b) the wrong land cover information provided by ECOCLIMAP, and (c) the presence of RFI at L-band in the Maqu region (Dente et al., 2012a).

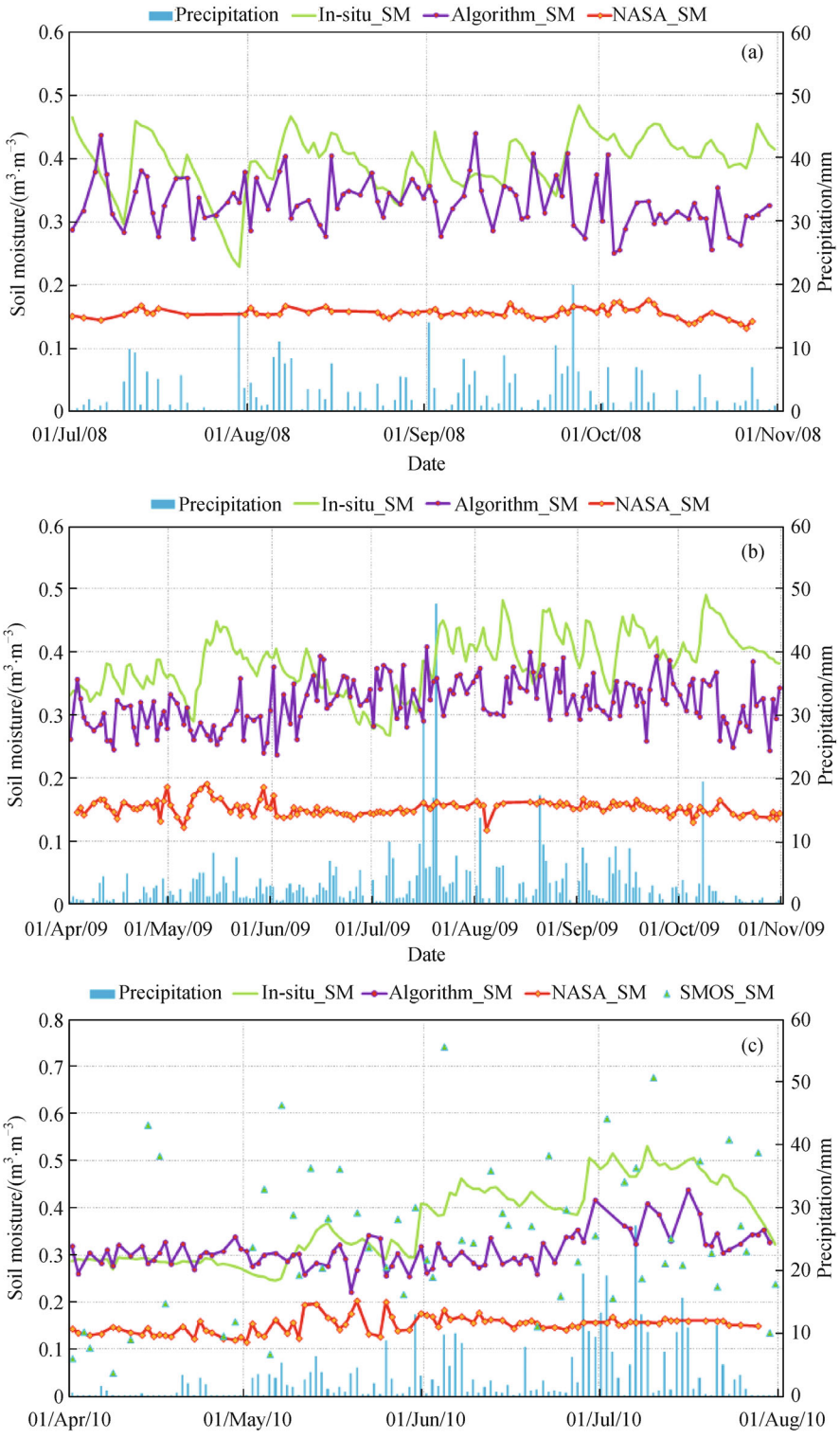

Fig. 5 Time series comparison of soil moisture retrieved by the present inversion algorithm and two satellite soil moisture products (NASA AMSR-E and SMOS) with in-situ average soil moisture at 5 cm. (a) 2008.7.1–2008.10.31; (b) 2009.4.1–2009.10.31; (c) 2010.4.1–2010.7.31.

The deviation between the Algorithm_SM and In-situ_SM may be caused by different spatial observation scales between in-situ points and satellite pixels. In addition, the bias may also be caused by the mismatch

Table 1 Error statistics of Algorithm_SM, NASA_SM, and SMOS_SM, with respect to the In-situ_SM.

Period of comparison	STD				Bias			MAE			RMSE		
	In-situ _SM	Algorithm _SM	NASA _SM	SMOS _SM	Algorithm _SM	NASA _SM	SMOS _SM	Algorithm _SM	NASA _SM	SMOS _SM	Algorithm _SM	NASA _SM	SMOS _SM
2008.7.1–2008.10.31	0.046	0.041	0.009	/	–0.066	–0.248	/	0.078	0.248	/	0.093	0.25	/
2009.4.1–2009.10.31	0.047	0.039	0.012	/	–0.064	–0.229	/	0.074	0.229	/	0.088	0.233	/
2010.4.1–2010.7.31	0.082	0.036	0.018	0.155	–0.054	–0.217	–0.039	0.069	0.217	0.133	0.086	0.23	0.14
All	0.059	0.04	0.013	/	–0.062	–0.230	/	0.074	0.23	/	0.088	0.236	/

STD (Standard deviation), Bias, MAE (Mean absolute error), RMSE (Root mean square error) are in $m^3 \cdot m^{-3}$.

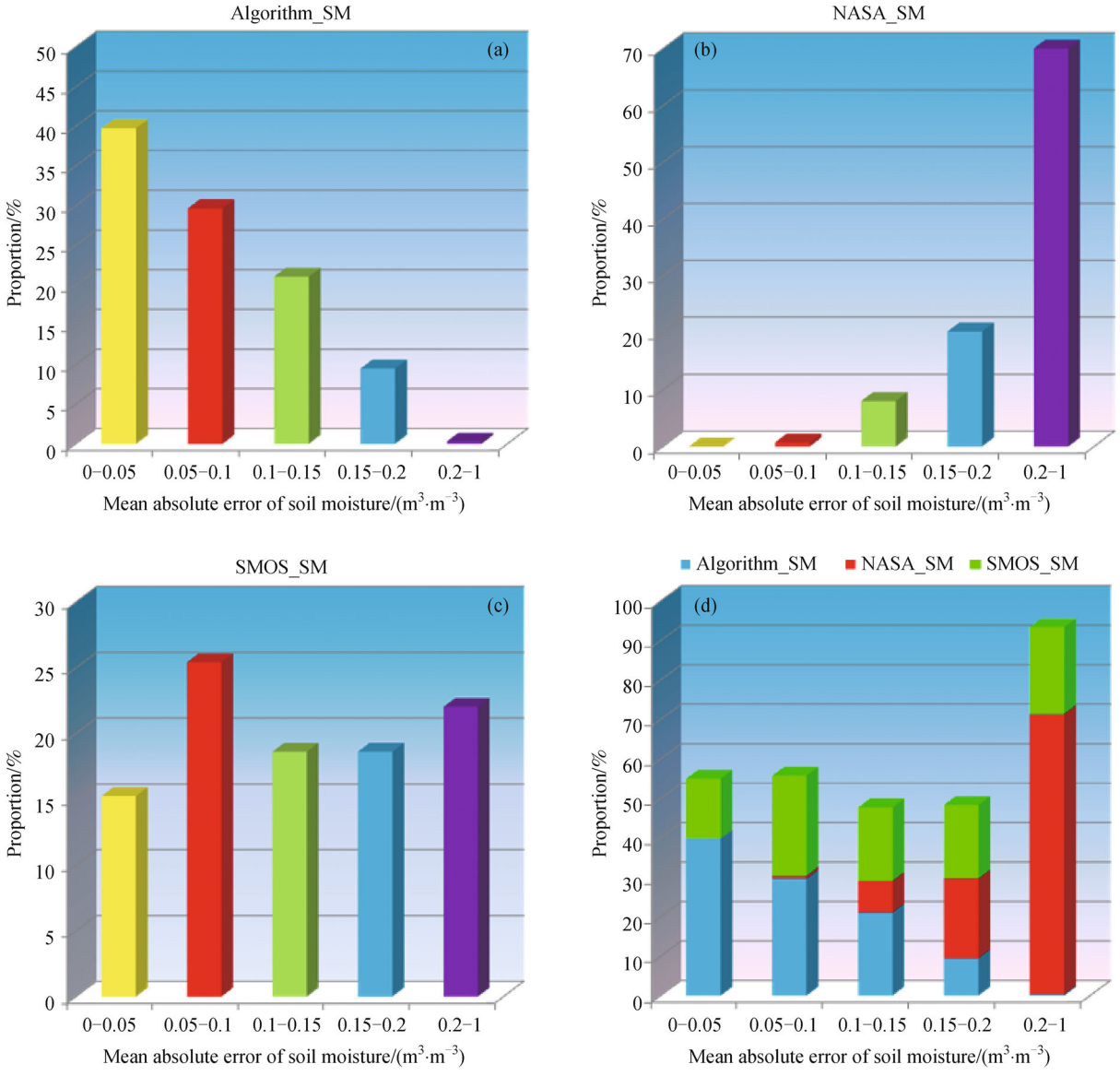

Fig. 6 Histogram of the distribution of mean absolute error between in-situ soil moisture, at 5 cm, and estimated soil moisture. (a) Algorithm_SM; (b) NASA_SM; (c) SMOS_SM; (d) all of three soil moisture retrievals.

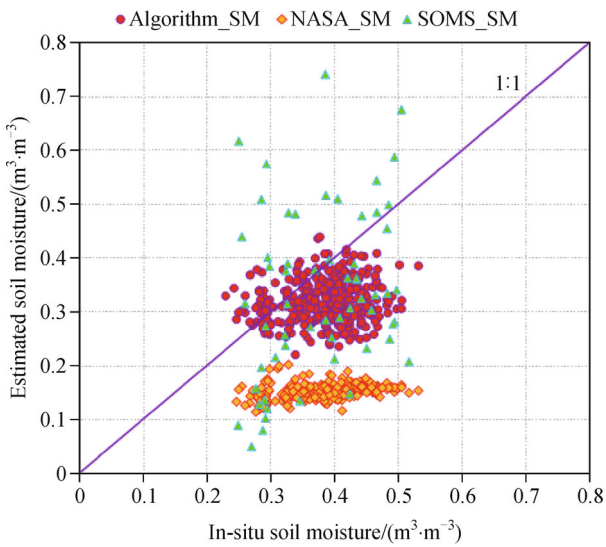

Fig. 7 Scatter plots comparison of soil moisture retrieved by the present inversion algorithm and two satellite soil moisture products (NASA AMSR-E and SMOS) with in-situ average soil moisture at 5 cm during the entire period.

between the in-situ soil moisture measuring depth and the microwave penetration depth. Certainly, these two factors are also error sources that influence the AMSR-E and SMOS products. Furthermore, the assumptions in the algorithm for simplifying the inversion process may also introduce errors. The complex topography in the Tibetan Plateau was not considered in the algorithm, which may be another error source. Considering the assumptions in the algorithm, the following cases should be noted when using the proposed algorithm: (a) it is only applicable in regions without strong RFI and is more suitable at lower microwave frequencies, and (b) both H and V polarized brightness temperature observations should be provided in order to use MPDI.

Some researchers have also developed prominent soil moisture algorithms for the Tibetan Plateau (Wen et al., 2003; Zhao et al., 2011b), but in these algorithms ancillary data, such as roughness or soil moisture, are needed as calibration parameters, and multi-frequency brightness temperature data is also necessary during the retrieval process. In contrast, the proposed algorithm uses observations of brightness temperature at only one frequency, and uses the least auxiliary data, namely soil texture, during the whole soil moisture retrieval process.

In general, the methodology presented in this study has much higher accuracy when compared with the other two satellite retrieval algorithms used in the Tibetan Plateau, although the NASA AMSR-E and SMOS algorithms are not designed to work in Tibetan Plateau regions. Moreover, since the proposed algorithm is physically-based instead of using the empirical relationship, it has no regional dependence and is more robust than the NASA AMSR-E official algorithm. In comparison with the SMOS official algorithm, the proposed algorithm has no reliance on ancillary vegetation data sets, which are very difficult to obtain globally, thus it can be applied more conveniently. Indeed, the inversion results of all three algorithms in the Maqu are not very satisfactory, especially the correlation coefficient between estimated and in-situ soil moisture, which is not very high. Two explanations for this are possible. One is that the Tibetan plateau is a very complex region with high spatial heterogeneity (Xie et al., 2010), which will bring large uncertainties for the validation of soil moisture retrieval algorithms. The other is that there are inherent limitations in all of the inversion algorithms due to the simplifications that are required for implementation (Jackson et al., 2010). These algorithms are based on the same radiative transfer model. However, each algorithm has to make some assumptions and apply various parameterized methods due to a lack of measured data, e.g., assuming the vegetation single scattering albedo to be constant, or using the empirical relationship to obtain the vegetation optical thickness. These simplifications will definitely bring some errors. Thus, it is indicated that there is still much work to do to make further improvements to the satellite retrieval algorithms.

5 Conclusions

A simplified physically-based algorithm developed for surface soil moisture retrieval from satellite microwave radiometer data is presented. The influence of both surface roughness and vegetation is grouped into a single parameter in the proposed algorithm. Furthermore, different from previous methods, which usually used the 37 GHz vertical polarized brightness temperature to obtain surface temperature (De Jeu and Owe, 2003; Holmes et al., 2009), this approach uses the MPDI to eliminate the effects of temperature, and obtains soil moisture through a nonlinear iterative procedure of minimizing the absolute value of the differences between the simulated and observed MPDI. Therefore, the present method needs only single-frequency brightness temperature observations and uses the least auxiliary data, namely soil texture, during the whole soil moisture retrieval process.

Due to the low attenuation from clouds and vegetation, as well as rarely occurring RFI at C-band in the Tibetan Plateau, the 6.9 GHz dual-polarized brightness temperature data from AMSR-E were selected for soil moisture estimation. Since the soil and vegetation canopy temperatures are in greater equilibrium during nighttime, only nighttime data were used. The observations of frozen soil were excluded in the study to reduce the uncertainty introduced by converting the dielectric constant into soil moisture. In-situ data collected from 20 sites of the Maqu soil moisture monitoring network were used to evaluate soil moisture in a long time series comparison between soil moisture data retrieved by the present algorithm, and both

the NASA soil moisture products and SMOS soil moisture products. The results show that the Algorithm_SM displays stronger agreement with ground measurements in temporal variations than the other two methods. The NASA products and SMOS products fail to capture the dynamics of in-situ data, with a larger RMSE of 0.235 $m^3 \cdot m^{-3}$ and 0.140 $m^3 \cdot m^{-3}$, respectively. The comparison also demonstrates that the proposed algorithm is an effective method for soil moisture retrieval that can significantly improve the estimation accuracy of soil moisture compared to NASA's and SMOS's algorithm in the Tibetan Plateau.

In this study, the same value of the polarization mixing parameter Q calibrated by Njoku and Chan (2006) at 6.9 GHz was adopted. At lower frequencies, such as L band, the Q value becomes much smaller, and thus can be reasonably negligible (Wigneron et al., 2001). Besides, the assumption in the algorithm that the single scattering albedo is equal to zero is also more reasonable at this band. Thus, in theory, the present method may also be applied to soil moisture inversion in the SMOS satellite mission and the SMAP mission with slight adjustments, but its applicability on these missions needs to be validated.

Acknowledgements We are grateful to Dr. Alok Sahoo from Princeton University for his valuable assistance, and professor Yang Kun from the Institute of Tibetan Plateau Research, Chinese Academy of Sciences, for kindly providing the precipitation data. We also thank NSIDC, CATDS (Centre Aval de Traitement des Données SMOS), and the International Soil Moisture Network for providing the AMSR-E products, SMOS products, and in-situ soil moisture data, respectively. This work was supported by the Chinese Ministry of Science and Technology (No. 2011AA120403), the Director Foundation for Postgraduates of Institute of Remote Sensing and Digital Earth Chinese Academy of Sciences (No. Y3ZZ17101B), and partially supported by the National Natural Science Foundation of China (Grant No. 41101391) and the Key Laboratory of Mapping from Space, National Administration of Surveying, Mapping and Geoinformation (No. K201301).

References

Anterrieu E, Khazaal A (2011). One year of RFI detection and quantification with L1a signals provided by SMOS reference radiometers. In: Proceedings of IEEE International Geoscience and Remote Sensing Symposium (IGARSS), 2245–2248

Becker F, Choudhury B J (1988). Relative sensitivity of normalized difference vegetation index (NDVI) and microwave polarization difference index (MPDI) for vegetation and desertification monitoring. Remote Sens Environ, 24(2): 297–311

Berthon L, Mialon A, Cabot F, Bitar A A, Richaume P, Kerr Y, Leroux D, Bircher S, Lawrence H, Quesney A, Jacquette E (2012). CATDS level 3 data product description. CESBIO-SA Technical Report

Chen L, Shi J C, Wigneron J P, Chen K S (2010). A parameterized surface emission model at L-band for soil moisture retrieval. IEEE Geosci Remote Sens Lett, 7(1): 127–130

Chen Y Y, Yang K, Qin J, Zhao L, Tang W J, Han M L (2013). Evaluation of AMSR-E retrievals and GLDAS simulations against observations of a soil moisture network on the central Tibetan plateau. J Geophys Res, D, Atmospheres, 118, doi: 10.1002/jgrd.50301

De Jeu R A M, Owe M (2003). Further validation of a new methodology for surface moisture and vegetation optical depth retrieval. Int J Remote Sens, 24(22): 4559–4578

Dente L, Su Z B, Wen J (2012a). Validation of SMOS soil moisture products over the Maqu and Twente regions. Sensors (Basel), 12(8): 9965–9986

Dente L, Vekerdy Z, Wen J, Su Z B (2012b). Maqu network for validation of satellite-derived soil moisture products. Int J Appl Earth Obs Geoinf, 17: 55–65

Draper C S, Walker J P, Steinle P J, De Jeu R A M, Holmes T R H (2009). An evaluation of AMSR-E derived soil moisture over Australia. Remote Sens Environ, 113(4): 703–710

Du J Y (2012). A method to improve satellite soil moisture retrievals based on Fourier analysis. Geophys Res Lett, 39(15): L15404, doi: 10.1029/2012GL052435

Entekhabi D, Njoku E, O'Neill P E, Kellogg K H, Crow W T, Edelstein W N, Entin J K, Goodman S D, Jackson T J, Johnson J, Kimball J, Piepmeier J R, Koster R D, Martin N, McDonald K C, Moghaddam M, Moran S, Reichle R, Shi J C, Spencer M W, Thrman S W, Tsang L, van Zyl J (2010). The soil moisture active passive (SMAP) mission. Proc IEEE, 98(5): 704–716

Guo P, Shi J C, Liu Q, Du J Y (2013). A new algorithm for soil moisture retrieval with L-band radiometer. IEEE J Sel Top Appl Farth Observ Remote Sens, 6(3): 1147–1155

Hallikainen M T, Ulaby F T, Dobson M C, El-Rayes M A, Wu L K (1985). Microwave dielectric behavior of wet soil-part 1: empirical models and experimental observations. IEEE Trans Geosci Rem Sens, GE-23(1): 25–34

Holmes T R H, De Jeu R A M, Owe M, Dolman A J (2009). Land surface temperature from Ka band (37 GHz) passive microwave observations. J Geophys Res, 114(D4): D04113

Hong S (2010). Global retrieval of small-scale roughness over land surfaces at microwave frequency. J Hydrol (Amst), 389(1–2): 121–126

Jackson T J (1993). Measuring surface soil moisture using passive microwave remote sensing. Hydrol Processes, 7(2): 139–152

Jackson T J, Cosh M H, Bindlish R, Starks P J, Bosch D D, Seyfried M, Goodrich D C, Moran M S, Du J Y (2010). Validation of Advanced Microwave Scanning Radiometer soil moisture products. IEEE Trans Geosci Rem Sens, 48(12): 4256–4272

Jackson T J, Hawley M E, O'Neill P E (1987). Preplanting soil moisture using passive microwave sensors. J Am Water Resour Assoc, 23(1): 11–19

Jackson T J, Le Vine D M, Hsu A Y, Oldak A, Starks P J, Swift C T, Isham J, Haken M (1999). Soil moisture mapping at regional scales using microwave radiometry: the southern Great Plains hydrology experiment. IEEE Trans Geosci Rem Sens, 37(5): 2136–2151

Jacquette E, Al Bita A, Mialon A, Kerr Y, Quesney A, Cabot F, Richaume P (2010). SMOS CATDS level 3 global products over land. Proc SPIE, 7824: 78240K, 78240K-6

Jin R, Li X, Che T (2009). A decision tree algorithm for surface soil freeze/thaw classification over China using SSM/I brightness temperature. Remote Sens Environ, 113(12): 2651–2660

Kerr Y H, Waldteufel P, Wigneron J P, Martinuzzi J, Font J, Berger M (2001). Soil moisture retrieval from space: the soil moisture and ocean salinity (SMOS) mission. IEEE Trans Geosci Rem Sens, 39(8): 1729–1735

Koike T, Nakamura Y, Kaihotsu I, Davaa G, Matsuura N, Tamagawa K, Fujii H (2004). Development of an advanced microwave scanning radiometer (AMSR-E) algorithm of soil moisture and vegetation water content. Annu J Hydraul Eng, JSCE, 48: 217–222

Lacava T, Coviello I, Faruolo M, Mazzeo G, Pergola N, Tramutoli V (2013). A multitemporal investigation of AMSR-E C-band radio-frequency interference. IEEE Trans Geosci Rem Sens, 51(4): 2007–2015

Lu H, Shi J C (2012). Reconstruction and analysis of temporal and spatial variations in surface soil moisture in China using remote sensing. Chin Sci Bull, 57(22): 2824–2834

Mao K B, Tang H J, Zhang L X, Li M C, Guo Y, Zhao D Z (2008). A method for retrieving soil moisture in Tibet region by utilizing microwave index from TRMM/TMI data. Int J Remote Sens, 29(10): 2903–2923

Meesters A G, De Jeu R A M, Owe M (2005). Analytical derivation of the vegetation optical depth from the microwave polarization difference index. IEEE Geosci Remote Sens Lett, 2(2): 121–123

Mladenova I, Lakshmi V, Jackson T J, Walker J P, Merlin O, De Jeu R A M (2011). Validation of AMSR-E soil moisture using L-band airborne radiometer data from National Airborne Field Experiment 2006. Remote Sens Environ, 115(8): 2096–2103

Mo T, Choudhury B J, Schmugge T J, Wang J R, Jackson T J (1982). A model for microwave emission from vegetation-covered fields. J Geophys Res, 87(C13): 11229–11237

Njoku E G, Ashcroft P, Chan T K, Li L (2005). Global survey and statistics of radio-frequency interference in AMSR-E land observations. IEEE Trans Geosci Rem Sens, 43(5): 938–947

Njoku E G, Chan S K (2006). Vegetation and surface roughness effects on AMSR-E land observations. Remote Sens Environ, 100(2): 190–199

Njoku E G, Entekhabi D (1996). Passive microwave remote sensing of soil moisture. J Hydrol (Amst), 184(1–2): 101–129

Njoku E G, Jackson T J, Lakshmi V, Chan T K, Nghiem S V (2003). Soil moisture retrieval from AMSR-E. IEEE Trans Geosci Rem Sens, 41 (2): 215–229

Owe M, De Jeu R A M, Holmes T R H (2008). Multisensor historical climatology of satellite-derived global land surface moisture. J Geophys Res, 113(F1): F01002

Paloscia S, Macelloni G, Santi E (2006). Soil moisture estimates from AMSR-E brightness temperatures by using a dual-frequency algorithm. IEEE Trans Geosci Rem Sens, 44(11): 3135–3144

Paloscia S, Pampaloni P (1988). Microwave polarization index for monitoring vegetation growth. IEEE Trans Geosci Rem Sens, 26(5): 617–621

Reynolds C A, Jackson T J, Rawls W J (2000). Estimating soil water-holding capacities by linking the food and agriculture organization soil map of the world with global pedon databases and continuous pedotransfer functions. Water Resour Res, 36(12): 3653–3662

Roy A, Royer A, Wigneron J P, Langlois A, Bergeron J, Cliche P (2012). A simple parameterization for a boreal forest radiative transfer model at microwave frequencies. Remote Sens Environ, 124: 371–383

Rüdiger C, Calvet J C, Gruhier C, Holmes T R H, De Jeu R A M, Wagner W (2009). An intercomparison of ERS-Scat and AMSR-E soil moisture observations with model simulations over France. J Hydrometeorol, 10(2): 431–447

Saha S K (1995). Assessment of regional soil moisture conditions by coupling satellite sensor data with a soil-plant system heat and moisture balance model. Int J Remote Sens, 16(5): 973–980

Saleh K, Wigneron J P, de Rosnay P, Calvet J C, Kerr Y (2006). Semi-empirical regressions at L-band applied to surface soil moisture retrievals over grass. Remote Sens Environ, 101(3): 415–426

Santi E, Pettinato S, Paloscia S, Pampaloni P, Macelloni G, Brogioni M (2012). An algorithm for generating soil moisture and snow depth maps from microwave spaceborne radiometers: HydroAlgo. Hydrol Earth Syst Sci, 16(10): 3659–3676

Shi J C, Jackson T, Tao J, Du J, Bindlish R, Lu L, Chen K S (2008). Microwave vegetation indices for short vegetation covers from satellite passive microwave sensor AMSR-E. Remote Sens Environ, 112(12): 4285–4300

Shi J C, Jiang L M, Zhang L X, Chen K S, Wigneron J P, Chanzy A, Jackson T J (2006). Physically based estimation of bare-surface soil moisture with the passive radiometers. IEEE Trans Geosci Rem Sens, 44(11): 3145–3153

Skou N, Misra S, Balling J E, Kristensen S S, Sobjaerg S S (2010). L-band RFI as experienced during airborne campaigns in preparation for SMOS. IEEE Trans Geosci Rem Sens, 48(3): 1398–1407

Su Z, Wen J, Dente L, van der Velde R, Wang L, Ma Y, Yang K, Hu Z (2011). The Tibetan Plateau observatory of plateau scale soil moisture and soil temperature (Tibet-Obs) for quantifying uncertainties in coarse resolution satellite and model products. Hydrol Earth Syst Sci, 15(7): 2303–2316

Van de Griend A A, Owe M (1994). Microwave vegetation optical depth and inverse modelling of soil emissivity using Nimbus/SMMR satellite observations. Meteorol Atmos Phys, 54(1–4): 225–239

Wagner W, Naeimi V, Scipal K, de Jeu R A M, Martínez-Fernández J (2007). Soil moisture from operational meteorological satellites. Hydrogeol J, 15(1): 121–131

Wang J R, Choudhury B J (1981). Remote sensing of soil moisture content over bare fields at 1.4 GHz frequency. J Geophys Res, 86 (C6): 5277–5282

Wang L L, Qu J J (2009). Satellite remote sensing applications for surface soil moisture monitoring: a review. Front Earth Sci China, 3 (2): 237–247

Wen J, Su Z B, Ma Y M (2003). Determination of land surface temperature and soil moisture from tropical rainfall measuring mission/microwave imager remote sensing data. J Geophys Res, 108 (D2): 4038

Wigneron J P, Calvet J C, Pellarin T, Van de Griend A A, Berger M, Ferrazzoli P (2003). Retrieving near-surface soil moisture from microwave radiometric observations: current status and future plans. Remote Sens Environ, 85(4): 489–506

Wigneron J P, Laguerre L, Kerr Y H (2001). A simple parameterization of the L-Band microwave emission from rough agricultural soils. IEEE Trans Geosci Rem Sens, 39(8): 1697–1707

Xie H, Ye J S, Liu X M, E C Y (2010). Warming and drying trends on the Tibetan Plateau (1971–2005). Theor Appl Climatol, 101(3–4): 241–

253

Zhang X F, Zhao J P, Sun Q, Wang X Y, Guo Y L, Li J (2011). Soil moisture retrieval from AMSR-E data in Xinjiang (China): models and validation. IEEE J Sel Top Appl Earth Observ Remote Sens, 4 (1): 117–127

Zhao T J, Zhang L X, Jiang L M, Zhao S J, Chai L N, Jin R (2011a). A new soil freeze/thaw discriminant algorithm using AMSR-E passive microwave imagery. Hydrol Processes, 25(11): 1704–1716

Zhao T J, Zhang L X, Shi J C, Jiang L M (2011b). A physically based statistical methodology for surface soil moisture retrieval in the Tibet Plateau using microwave vegetation indices. J Geophys Res, 116 (D8): D08116